MicroGrid Resilience-Oriented Scheduling: A Robust MISOCP Model

Natalia-Maria Zografou-Barredo, Charalampos Patsios, *Member, IEEE*, Ilias Sarantakos, Peter Davison, Sara Louise Walker, and Philip C. Taylor, *Senior Member, IEEE*

***Abstract*—This article introduces a Robust Mixed-Integer Second Order Cone Programming (R-MISOCP) model for the resilience-oriented optimal scheduling of microgrids (MGs). This is developed for MGs that are islanded due to a scheduled interruption from the main grid, where minimizing both operational costs and load shedding is critical. The model introduced presents two main benefits. Firstly, an accurate second order cone power flow model (SOC-PF) is used, which ensures global optimality. Through a comparison with a piecewise linear power flow model on a modified IEEE 33 bus network, it is demonstrated that failure to accurately model power flow equations, can result in a significant underestimation of the operational cost of almost 12%. Secondly, uncertainty is modelled using a robust approach which allows trade-offs between the uncertainty that a MG operator is willing to tolerate, and performance. In this article, performance criteria considered are operational cost and load shedding. Market price, demand, renewable generation and islanding duration are considered as uncertain variables. Results show that by controlling the budget of uncertainty, the MG operator can achieve an almost 20% reduction in the operating cost, compared to a fully robust schedule, while achieving 0% probability of shedding more demand than expected.**

***Index Terms*—Islanding, microgrid optimal scheduling, mixed integer second order cone programming, resilience, robust optimization.**

NOMENCLATURE

Abbreviations

EV	Electric vehicle.
ESS	Energy storage system.
DER	Distributed energy resource.
DG	Dispatchable generator.
D − MISOCP	Deterministic mixed-integer second order cone programming.
MISOCP	Mixed-integer second order cone programming.
MG	MicroGrid.
PLS	Probability of load shedding.
PoU	Probability of underestimating operational cost.
PV	Photovoltaic.
PWL − PF	Piecewise linear power flow.
R − MISOCP	Robust mixed-integer second order cone programming.
RO	Robust optimization.
SOC − PF	Second order cone power flow.

Decision Variables

$D_{it}^{P/Q}$	Real/reactive demand at bus i at time t [MW], [MVar].
$D_{it}^{P/Q^{Shed}}$	Real/reactive demand not supplied [MW], [MVar].
$\boldsymbol{e}$	Binary variable for EV charge or discharge state.
$G_{it}^{P/Q}$	Total real and reactive power generated at bus i at time t [MW], [MVar].
$I_{ij,t}$	Squared current value of line $i-j$ at time t [kA^2].
$isl_t^{L/R}$	Binary variables stating MG grid-connected or islanded.
$P_{it}^{ESS,Ch/Dch}$	Charging/discharging power of ESS at bus i at time t [MW].
$P_{it}^{EV,Ch/Dch}$	Charging/discharging power of EV parking lot at bus i at time t [MW].
P_{it}^{DG}, Q_{it}^{DG}	DG output at bus i at time t [MW], [MVar].
P_t^{Grid}, Q_t^{Grid}	Real/Reactive power imported from the utility grid [MW], [MVar].
$PF_{ij,t}^{P/Q}$	Power flow of branch $i-j$ at time t [MW], [MVar].
$SOC_{i,t}^{ESS}$	State of change of ESS at bus i at time t [MW].
SOC_{it}^{Sat}	EV parking lot state of change, associated with the CC to CV charging method for Li-ion batteries.
$\boldsymbol{u}$	Binary unit commitment decision.
V_{it}	Squared voltage value at bus i at time t [kV^2].
$\boldsymbol{x}^{ESS}$, $\boldsymbol{y}^{ESS}$	Binary variables for ESS Charging/Discharging state.

Manuscript received February 24, 2020; revised June 23, 2020, August 20, 2020 and October 23, 2020; accepted October 27, 2020. Date of publication November 20, 2020; date of current version April 21, 2021. This work was supported in part by Newcastle University and the EPSRC National Center for Energy Systems Integration (CESI) under Grant EP/P001173/1, and in part by the EPSRC Multi-Scale Analysis for Facilities for Energy Storage (Manifest) under Grant EP/N032888/1. Paper no. TSG-00275-2020. *(Corresponding author: Natalia-Maria Zografou-Barredo.)*

Natalia-Maria Zografou-Barredo, Charalampos Patsios, Ilias Sarantakos, and Sara Louise Walker are with the School of Engineering, Newcastle University, Newcastle upon Tyne NE1 7RU, U.K. (e-mail: n.zografou-barredo2@newcastle.ac.uk).

Peter Davison is with the School of Electrical and Electronic Engineering, Newcastle University, Newcastle upon Tyne NE1 7RU, U.K.

Philip C. Taylor is with the University of Bristol, Bristol BS8 1TL, U.K.

Color versions of one or more figures in this article are available at https://doi.org/10.1109/TSG.2020.3039713.

Digital Object Identifier 10.1109/TSG.2020.3039713

$\boldsymbol{p}, \boldsymbol{z}, \boldsymbol{\varphi}, \boldsymbol{x}, \boldsymbol{y}, \boldsymbol{\omega}$	Variables of the robust formulation.
$\gamma^{\widetilde{I},Left}$, $\gamma^{\widetilde{I},Right}$	Integer variables stating the additional time periods that the MG is islanded, before the start-time and after the end-time of the scheduled islanding event, respectively.
θ_{it}	Voltage angle at bus i at time t.
$\omega_{ij,t}^{PWL}$	Tangent line for the piecewise linearization of $cos(\theta_{it} - \theta_{jt})$.

Indices

i, j, k, t	Indexing for parameters and decision variables.

Parameters

a_i, b_i	DG cost function parameters at bus i [£], [£/MWh].
$\{c, d, e, \boldsymbol{\beta}, \boldsymbol{\delta}, \boldsymbol{\vartheta}, \varkappa, \boldsymbol{\lambda}\}$	Auxiliary parameters for the robust formulation.
C_i^{max}	Maximum capacity of ESS unit at bus i.
$c_{i,t}^{Shed}$	Cost for shedding loads at bus i at time t [£/MWh].
c_{SU_i}, c_{SD_i}	Generator i start-up/shut-down cost [£].
$\overline{D_{it}^{P/Q}}$	Expected real/reactive demand at bus i at time t [MW], [MVar].
d_n, h_n	Constants used for the n linear segments of the piecewise linear power flow approximation.
$\overline{E_{EV}}$	EV parking lot energy capacity [MWh].
g_{ij}, b_{ij}	Conductance and susceptance of branch $i-j$.
I_t	Expected MG islanding period. $I_t = 1$ when MG islanded. $I_t = 0$ otherwise.
m_t	Expected market price at time t [£/MWh].
P_{it}^{PV}	Expected PV generation at bus i at time t [MW].
r_{ij}, x_{ij}	Resistance/Reactance of branch $i-j$ [Ω].
RU_i, RD_i	Ramp-up/Ramp-down limits of generator at bus i [MW].
s_{it}^{EV}	EV parking lot schedule.
$soc_i^{arr/dep}$	EV parking lot arrival/departure SOC.
SU_{it}, SD_{it}	Binary start-up/shut-down status of generator at bus i at time t.
$t_{start}^{isl}, t_{end}^{isl}$	Expected islanding start/end time.
$\boldsymbol{\Gamma}$	Budget of uncertainty.
η_i	Efficiency of ESS, EV parking lot at bus i [%].

Sets

E	Set of network branches.
J_i	Set of columns at the ith constraint.
$\mathbb{Z}$	The set of all integers.
Ω_B	Set of network buses.
Ω_{ESS}	Set of ESSs.
Ω_G	Set of generators.
Ω_T	Set of time periods.

Symbols

$\_$, $\overline{\ }$	Lower/Upper limit symbols.

I. Introduction

A. Motivation

THE REQUIREMENT to meet zero CO_2 emissions in the electricity sector, restructuring of the electricity business, and technological developments in microgeneration, have set a new paradigm of power systems in modern societies [1], [2]. Advances in distributed generation units (microturbines, fuel cells, etc.) and distributed storage devices (energy storage systems (ESS), batteries, etc.) have formed the broader class of distributed energy resources (DERs). The connection of DERs at medium or low voltage distribution networks have increased the flexibility of network stakeholders over the past decades, shaping new concepts for the future smart grid; including the concept of MicroGrids.

MicroGrids (MG) are medium or low voltage distribution networks with distributed generation units, energy storage devices, and flexible loads [3]. A MG can be operated in an autonomous or non-autonomous way, forming two modes of operation: the islanded and the grid-connected mode. In the grid-connected mode, MGs operate connected to the distribution grid or simply main grid. In the islanded mode, supply from the main grid is interrupted, and the MG depends only on the on-site DERs in order to satisfy the required demand; if demand exceeds generation, loads need to be curtailed.

Resilience represents the ability of a power system to supply the demand in the face of an event that has a high impact and a low probability of occurring [4]. This type of events occurs when the main grid is not available, either due to a scheduled interruption, e.g., an upstream maintenance, or a foreseeable natural disaster such as a hurricane [4]–[6]. MGs present a practical solution to enhance power system resilience by decreasing the probability of load shedding [4]. Operating in islanded mode, the MG can supply local demand in case of a high-impact-low-probability event, when supply from the main grid may be interrupted from several minutes to several hours.

MG resilience merits are well-acknowledged by the academic community [7], [8]. In recent years, there is an increasing interest to provide a framework for the mathematical modelling of the resilience-oriented MG optimal scheduling problem. A literature review of relevant studies is the underlying theme of the following subsection.

B. Literature Review

In order for MGs to enhance power system resilience, this calls for methods that can handle disconnection and re-connection of a MG when power from the main grid is interrupted for an extended period of time. An early

attempt clearly tailored towards this path, was presented by A. Khodaei in 2014 in [4]. This study proposed an operational framework for a MG which operated in islanded mode for an extended period of time due to interruption of supply from the main grid, and was introduced as the *resiliency-oriented MicroGrid optimal scheduling*. The proposed operational framework was mathematically formulated as a robust optimization problem. However, power flow equations were not included in the model, and robustness was treated in a conservative fashion; assuming maximum expected demand and minimum expected renewable generation at all times.

The study in [5], proposed a two-stage stochastic linear optimization model. In this model, unintentional islanding, load, pool price, and EV schedule were considered as random variables. Although power flow equations were included in the model, the formulation used did not have an accurate representation of network losses, which can result in a more optimistic outcome regarding the cost of operation. Additionally, the knowledge of the probability distributions of random variables is required in stochastic optimization. The latter can be a great advantage for a problem with well-known historical data. However, this is a limitation for modelling islanding uncertainty due to an interruption of power supply from the main grid, as this belongs to high-impact/low-probability events (HILP) for which historical data is rare [6], [9].

The study in [6], presented a two-stage robust optimization model. Load, market price, and the scheduled time of the MG islanding event were considered as uncertain parameters in this model. However, power flow equations were approximated.

The studies in [10], [11], presented resilient operation strategies for an AC/DC MG and a multi-energy MG respectively. The proposed models were mathematically formulated as two-stage robust optimization problems. In these studies, power flow equations were not considered at all in the network model, which creates the risk of overloading network lines, i.e., violating voltage or line current limits.

Finally, the study in [12], presented a model to enhance resilience using islanded operation of MGs focusing on the event of inadequate on-site generation to feed all MG loads. The model was mathematically formulated as a nonlinear programming problem. However, the proposed model was not formulated as a convex model, which meant that only a local optimal solution was guaranteed.

To conclude the above: the scientific community has proposed models for optimal scheduling of MGs that either lacked an accurate representation of power flow equations, or did not take into consideration power flow equations in their models. Furthermore, previous studies did not incorporate all prevailing uncertainties (such as pool price and islanding event uncertainty) which are necessary to form the resiliency-oriented scheduling for MGs (for further reading see the analysis in [6] and references therein). Finally, proposed models that accurately consider power flow equations, are non-convex, and therefore can only guarantee a local optimal solution.

C. Contribution and Organization of the Article

This research, proposes a Robust Mixed-Integer Second Order Cone Programming (R-MISOCP) model for the resilience-oriented optimal scheduling of MGs. The developed model captures the benefits of both convexity and robustness.

The contributions of this work are summarized as follows.

1) The Second Order Cone Power Flow (SOC-PF) model proposed in [13] is used to model power flow equations. This formulation is an exact convex approximation of the power flow model. To evaluate the performance of the R-MISOCP model, a detailed comparison is provided with a model that uses a piecewise linear power flow model (PWL-PF) which has been used in relevant MG studies.
2) Robust optimization is used to model uncertain data. Data uncertainty is considered in market price, demand, renewable generation (PV generation) and islanding duration. The robust approach of [14] is employed. This approach allows the MG operator to control the trade-off between tolerance of uncertainty and operating performance, using a parameter Γ called the budget of uncertainty. In this article, performance is assessed based on both cost of operation and load shedding.

In terms of the first contribution, computational experiments show that an AC power flow model that fails to accurately account for power flow equations, can result in a significant underestimation of both the operational costs, and the curtailed demand, and consequently lead to significantly different scheduling decisions. Regarding the second contribution, computational experiments show that, for the MG under study, the MG operator can adjust the budgets of uncertainty, and achieve a sizable reduction in the day-ahead operational costs, compared to a fully robust (conservative) approach, while having a 0% probability of shedding additional loads than expected.

The remainder of this article is organized as follows. Section II, presents the employed robust approach. Section III, presents the proposed R-MISOCP model and the underlying deterministic model. Section IV, shows computational experiments and discussion. Section V, presents the conclusions of this research.

II. Modelling Under Data Uncertainty

Optimization problems can be formed using data that are not known with certainty. Robust optimization (RO) is an approach to optimization under uncertainty, where the solution is immunized against any realization of the uncertain parameters which belong to a deterministic interval [15]. The motivation and goals of this approach are twofold. First, in RO, data uncertainty is not stochastic and distribution information is not needed. Second, the RO formulation of an important class of optimization problems (such as linear and second-order cone programming problems [15]) is computationally tractable.

In the day-ahead scheduling problem for MGs, being fully robust, i.e., considering the *worst* possible case of uncertainty, may be too conservative, in the sense that too much of the performance may be sacrificed in order to be able to tolerate any possible perturbation of the uncertain data. For

the resilience-oriented MG day-ahead scheduling considered in this article, performance criteria include both operational cost and load shedding levels. The robust approach of [14] is employed, where the trade-off between tolerance of uncertainty and model performance can be controlled with a parameter Γ, called the budget of uncertainty. This parameter allows the MG operator to control the cost of operation and load shedding levels, while being robust against possible data perturbations with a very high probability.

In this article, the MG day-ahead scheduling problem is formulated as an MISOCP optimization problem with uncertain data. The robust approach of [14] is employed to the problem (1a)-(1e), where data uncertainty only exists in the linear constraints (1b). The robust model that is proposed in Section III is formulated accordingly.

Consider the following deterministic MISOCP problem:

$$\min \quad c^T \boldsymbol{x} + d^T \boldsymbol{\varphi} + e^T \boldsymbol{\omega} \tag{1a}$$

subject to

$$\sum_j \lambda_{ij} x_j + \sum_j \beta_{ij} \varphi_j + \sum_j \delta_{ij} \omega_j \leq \eta_i \quad \forall i \tag{1b}$$

$$\varkappa^T \boldsymbol{\varphi} \geq \left\| \vartheta \boldsymbol{\varphi} \right\|_2 \tag{1c}$$

$$\underline{\boldsymbol{x}} \leq \boldsymbol{x} \leq \overline{\boldsymbol{x}}, \quad \underline{\boldsymbol{\varphi}} \leq \boldsymbol{\varphi} \leq \overline{\boldsymbol{\varphi}} \tag{1d}$$

$$\boldsymbol{x}, \boldsymbol{\varphi} \quad \text{continuous}, \quad \boldsymbol{\omega} \quad \text{binary} \tag{1e}$$

Assume that the coefficients λ_{ij} are uncertain, and each entry is a bounded and symmetric random variable $\widetilde{\lambda}_{ij}$ that takes values in $[\lambda_{ij} - \hat{\lambda}_{ij}, \lambda_{ij} + \hat{\lambda}_{ij}]$. Employing the robust approach of [14], the robust counterpart of problem (1a)–(1e) becomes as follows.

$$\min \quad c^T \boldsymbol{x} + d^T \boldsymbol{\varphi} + e^T \boldsymbol{\omega} \tag{2a}$$

subject to (1c)–(1d), and

$$\left[\sum_j \lambda_{ij} x_j + z_i \Gamma_i + \sum_j p_{ij} \right] + \sum_j \beta_{ij} \varphi_j + \sum_j \delta_{ij} \omega_j \leq \eta_i \quad \forall i \tag{2b}$$

$$z_i + p_{ij} \geq \hat{\lambda}_{ij} y_j, \quad -y_j \leq x_j \leq y_j \tag{2c}$$

$$\boldsymbol{z} \geq 0, \boldsymbol{p} \geq 0, \boldsymbol{y} \geq 0 \tag{2d}$$

$$\boldsymbol{x}, \boldsymbol{\varphi}, \boldsymbol{z}, \boldsymbol{p}, \boldsymbol{y} \quad \text{continuous}, \quad \boldsymbol{\omega} \quad \text{binary} \tag{2e}$$

where $j \in J_i$, $\Gamma_i \in [0, |J_i|]$, and z_i, p_{ij}, y_j decision variables that result from the robust formulation of [14].

III. Model

A. Description

This study presents a model for the optimal scheduling problem of MGs that are islanded for an extended and uncertain period of time. The proposed model is mathematically formulated as a robust mixed-integer second-order cone problem. Uncertain parameters are modelled using the robust optimization approach proposed in [14], as presented in the preceding section.

The model has binary and continuous decision variables. Binary decision variables represent: unit commitment decisions, charging/discharging state of the energy storage system (ESS), charging/discharging state of the electric vehicle (EV) parking lot, and the state of connection between the MG and the main grid (grid-connected/islanded). Continuous decision variables represent: scheduling of MG assets (DGs, charged/discharged power of ESS and EV parking lot), imported power from the main grid, bus voltages, power flows, line losses, ESS state-of-charge, loads (fixed and curtailed), and auxiliary decision variables as a result of the robust formulation.

The objective of the R-MISOCP model is to minimize the MG cost of operation. The cost of operation includes: DG generation cost (using DG cost functions), start-up/shut-down costs, the cost to buy power from the main grid, and the cost for load shedding when (during the islanded operation) there is insufficient generation to feed the demand. Constraints represent: the SOC-PF model, branch current limits, unit commitment decisions, ramp-up/down limits, the ESS model, the EV parking lot model, and upper/lower limits of variables (namely of fixed loads, curtailable loads, bus voltage, DGs and grid power). The EV parking lot is modelled as an aggregated EV, using the set of linear constraints (9a) - (9h) [5], [16], where constraints (9a), (9b) represent the arrival and departure SOC respectively. The EVs follow the CC to CV (Constant Current to Constant Voltage) charging method for Li-ion batteries, presented in the Appendix of [16]. Data for the parameters related to the EV parking lot are presented in Table VIII-Appendix A of this manuscript.

The following subsections present the mathematical formulation of the underlying deterministic model, and the proposed robust model, respectively.

B. Deterministic Model (D-MISOCP)

The deterministic model is mathematically formulated as an MISOCP problem and is presented in equations (3)–(14b).

$$\min \sum_{i \in \Omega_G} \sum_{t \in \Omega_T} \left(b_i P_{it}^{DG} + a_i u_{it} + c_{SU_i} SU_{it} + c_{SD_i} SD_{it} \right) + \sum_{t \in \Omega_T} m_t P_t^{Grid} + \sum_{i \in \Omega_B} \sum_{t \in \Omega_T} c_{it}^{Shed} D_{it}^{P^{Shed}} \tag{3}$$

subject to

Power flow equations [13]$-\forall t \in \Omega_T$

$$PF_{ij,t}^P = \sum_{k:(j,k) \in E} PF_{jk,t}^P + r_{ij} I_{ij,t} + D_{jt}^P - G_{jt}^P \quad \forall (i,j) \in E \tag{4a}$$

$$G_{it}^P = \sum_{i \in \Omega_G} \Big[P_{it}^{DG} + P_{it}^{ESS,Dch} - P_{it}^{ESS,Ch} + P_{it}^{EV,Dch} - P_{it}^{EV,Ch} + P_t^{Grid} + P_{it}^{PV} + D_{it}^{P^{Shed}} \Big] \quad \forall i \in \Omega_B \tag{4b}$$

$$PF_{ij,t}^Q = \sum_{k:(j,k) \in E} PF_{jk,t}^Q + x_{ij} I_{ij,t} + D_{jt}^Q - G_{jt}^Q, \quad \forall (i,j) \in E \tag{4c}$$

$$G_{it}^Q = \sum_{i \in \Omega_G} \Big[Q_{it}^{DG} + Q_t^{Grid} + D_{it}^{Q^{Shed}} \Big] \quad \forall i \in \Omega_B \tag{4d}$$

$$PF_{ij,t}^P = P_t^{Grid}, \quad i : \text{Slack bus} \tag{4e}$$

$$PF_{ij,t}^Q = Q_t^{Grid}, \quad i : \text{Slack bus} \tag{4f}$$

$$V_{jt} = V_{it} - 2\left(r_{ij}\,PF^{P}_{ij,t} + x_{ij}\,PF^{Q}_{ij,t}\right) + \left(\left(r_{ij}\right)^2 + \left(x_{ij}\right)^2\right) I_{ij,t} \tag{4g}$$

$$I_{ij,t} + V_{it} \geq \left\| \left[2\,PF^{P}_{ij,t} \quad 2\,PF^{Q}_{ij,t} \quad (I_{ij,t} - V_{it}) \right]^T \right\|_2 \tag{4h}$$

Branch current limits$-\forall (i,j) \in E$

$$I_{ij,t} \leq \overline{I_{ij}} \tag{5a}$$

Unit commitment constraints$-\forall i \in \Omega_{ESS}\ \forall t \in \Omega_T$

$$u_{it} - u_{i(t-1)} \leq SU_{it}, \quad t \neq 1 \tag{6a}$$

$$u_{i(t-1)} - u_{it} \leq SD_{it}, \quad t \neq 1 \tag{6b}$$

$$\boldsymbol{u},\ \boldsymbol{SU},\ \boldsymbol{SD} \quad \text{binary}$$

Ramp-up/down limits$-\forall i \in \Omega_G\ \forall t \in \Omega_T$

$$P^{DG}_{it} - P^{DG}_{i(t-1)} \leq RU_i \tag{7a}$$

$$P^{DG}_{i(t-1)} - P^{DG}_{it} \leq RD_i \tag{7b}$$

Energy storage model$-\forall i \in \Omega_{ESS}\ \forall t \in \Omega_T$

$$SOC_{i(t=1)} = SOC_{i(t=T_{max})} \tag{7c}$$

$$SOC^{ESS}_{it} = SOC^{ESS}_{i(t-1)} + \left(\eta_i\,P^{ESS,Ch}_{it} - \frac{P^{ESS,Dch}_{it}}{\eta_i}\right)\Delta\tau \tag{8a}$$

$$\underline{SOC^{ESS}_{it}} \leq SOC^{ESS}_{it} \leq \overline{SOC^{ESS}_{it}} \tag{8b}$$

$$0 \leq P^{ESS,Ch}_{it} \leq x^{ESS}_{it}\,\overline{P^{ESS,Ch}_{it}} \tag{8c}$$

$$0 \leq P^{ESS,Dch}_{it} \leq y^{ESS}_{it}\,\overline{P^{ESS,Dch}_{it}} \tag{8d}$$

$$x^{ESS}_{it} + y^{ESS}_{it} \leq 1 \tag{8e}$$

$$\boldsymbol{x}^{ESS}, \boldsymbol{y}^{ESS} \quad \text{binary}$$

EV parking lot model [5], [16]$-\forall i \in \Omega_{EV_i}\ \forall t \in \Omega_T$

$$SOC^{EV}_{i(t=T_{arr})} = soc^{arr}_i\,\overline{E_{EV}}$$

$$SOC^{EV}_{i(t=T_{dep})} = soc^{dep}_i\,\overline{E_{EV}} \tag{9a}$$

$$SOC^{EV}_{it} = SOC^{EV}_{i(t-1)} + \left(\eta_i\,P^{EV,Ch}_{it} - \frac{P^{EV,Dch}_{it}}{\eta_i}\right)\Delta\tau \tag{9b}$$

$$0 \leq P^{EV}_{it} \leq s^{EV}_{it}\overline{P^{EV}_{it}} \tag{9c}$$

$$P^{EV}_{it} \leq \frac{\overline{P^{EV}_{it}}\,s^{EV}_{it}\,(1 - SOC_{it})}{\left(1 - SOC^{Sat}_{it}\right)} \tag{9d}$$

$$0 \leq P^{EV,Dch}_{it} \leq \overline{P^{EV,Dch}_{it}}\,e_{it} \tag{9e}$$

$$0 \leq P^{EV,Ch}_{it} \leq (1 - e_{it})\,\overline{P^{EV,Ch}_{it}} \tag{9f}$$

$$P^{EV}_{it} = P^{EV,Dch}_{it} + P^{EV,Ch}_{it} \tag{9g}$$

$$\boldsymbol{e} \quad \text{binary}$$

Fixed and curtailed demand limits [13]$-\forall i \in \Omega_B, t \in \Omega_T$

$$D^{P}_{it} \geq \underline{D^{P}_{it}}, \quad D^{Q}_{it} \geq \underline{D^{Q}_{it}} \tag{10a}$$

$$0 \leq D^{P^{Shed}}_{it} \leq \underline{D^{P}_{it}}, \quad 0 \leq D^{Q^{Shed}}_{it} \leq \underline{D^{Q}_{it}} \tag{10b}$$

Voltage limits$-\forall t \in \Omega_T$

$$\underline{V}_{it} \leq V_{it} \leq \overline{V}_{it}, \quad \forall i \in \Omega_B \tag{11a}$$

$$V_{it} = V^{Ref}_{it}, \quad i : \text{Slack bus} \tag{11b}$$

DG limits$-\forall t \in \Omega_T$

$$u_{it}\,\underline{P^{DG}_{it}} \leq P^{DG}_{it} \leq u_{it}\,\overline{P^{DG}_{it}} \quad \forall i \in \Omega_G \tag{12a}$$

$$u_{it}\,\underline{Q^{DG}_{it}} \leq Q^{DG}_{it} \leq u_{it}\,\overline{Q^{DG}_{it}} \quad \forall i \in \Omega_G \tag{12b}$$

Renewable generation limits$-\forall t \in \Omega_T$

$$P^{PV}_{it} \leq \overline{P^{PV}_{it}} \tag{13a}$$

Grid limits$-\forall t \in \Omega_T$

$$0 \leq P^{Grid}_{t} \leq \overline{P^{Grid}_{t}}\,(1 - I_t) \tag{14a}$$

$$0 \leq Q^{Grid}_{t} \leq \overline{Q^{Grid}_{t}}\,(1 - I_t). \tag{14b}$$

C. Robust Model (R-MISOCP)

The robust model is formulated as an MISOCP model and is presented in equations (15)–(22b) and (4c)–(13a). For the sake of succinctness, only constraints that are changed or added due to the robust formulation are presented in an extended way; equations (4c)–(13a) that are preserved are not re-written. In (4b),(4d) and (18b) $P^{Grid}_t = 0$, $Q^{Grid}_t = 0$ for buses i=2, 3, ...,

$$\min \quad \rho \tag{15}$$

subject to (4c)–(13a), and:

$$\rho \geq \sum_{i\in\Omega_G}\sum_{t\in\Omega_T}\left(b_i\,P^{DG}_{it} + a_i\,u_{it} + c_{SU_i}\,SU_{it} + c_{SD_i}\,SD_{it}\right) + \sum_{t\in\Omega_T} m_t\,P^{Grid}_t + z^{\widetilde{M}}\,\Gamma^{\widetilde{M}} + \sum_{t\in\Omega_T} p^{\widetilde{M}}_t + \sum_{i\in\Omega_B}\sum_{t\in\Omega_T} c^{Shed}_{it}\,D^{P^{Shed}}_{it} \tag{16}$$

Market price uncertainty$(\widetilde{\mathcal{M}})-\forall t \in \Omega_T$

$$z^{\widetilde{\mathcal{M}}} + p^{\widetilde{\mathcal{M}}}_t \geq \widehat{m}\,y^{\widetilde{\mathcal{M}}}_t \tag{17a}$$

$$-\,y^{\widetilde{\mathcal{M}}}_t \leq P^{Grid}_t \leq y^{\widetilde{\mathcal{M}}}_t,\ z^{\widetilde{\mathcal{M}}} \geq 0,\ p^{\widetilde{\mathcal{M}}}_t \geq 0,\ y^{\widetilde{\mathcal{M}}}_t \geq 0 \tag{17b}$$

$$\Gamma^{\widetilde{M}} \in [0, |\Omega_T|], \quad |\Omega_T| = 144 \tag{17c}$$

Power flow equations$-\forall t \in \Omega_T$

$$PF^{P}_{ij,t} = \sum_{k:(j,k)\in E} PF^{P}_{jk,t} + r_{ij}\,I_{ij,t} + D^{P}_{jt} + z^{\widetilde{D}}_t\,\Gamma^{\widetilde{D}}_t + p^{\widetilde{D}}_{jt} - G^{P}_{jt}, \forall (i,j) \in E \tag{18a}$$

$$G_{it}^{P} = \sum_{i\in\Omega_G}\Big[P_{it}^{DG} + P_{it}^{ESS,Dch} - P_{it}^{ESS,Ch} + P_{it}^{EV,Dch} - P_{it}^{EV,Ch} + P_{t}^{Grid} + P_{it}^{PV} - z_t^{\widetilde{RG}}\,\Gamma_t^{\widetilde{RG}} - p_{it}^{\widetilde{RG}} + D_{it}^{P^{Shed}}\Big], \quad \forall i \in \Omega_B \tag{18b}$$

Demand uncertainty$(\widetilde{\mathcal{D}}) - \forall t \in \Omega_T$

$$z_t^{\widetilde{D}} + p_{it}^{\widetilde{D}} \geq \widehat{d}\, y_{it}^{\widetilde{D}} \tag{19a}$$

$$-\, y_{it}^{\widetilde{D}} \leq D_{it}^{P} \leq y_{it}^{\widetilde{D}},\ z_t^{\widetilde{D}} \geq 0,\ p_{it}^{\widetilde{D}} \geq 0,\ y_{it}^{\widetilde{D}} \geq 0 \tag{19b}$$

$$\Gamma_t^{\widetilde{D}} \in [0, 1] \tag{19c}$$

Renewable generation uncertainty$(\widetilde{\mathcal{RG}}) - \forall t \in \Omega_T$

$$z_t^{\widetilde{RG}} + p_{it}^{\widetilde{RG}} \geq \widehat{g}\, y_{it}^{\widetilde{RG}} \tag{20a}$$

$$-\, y_{it}^{\widetilde{\mathcal{RG}}} \leq P_{it}^{RG} \leq y_{it}^{\widetilde{RG}},\ z_t^{\widetilde{\mathcal{RG}}} \geq 0,\ p_{it}^{\widetilde{\mathcal{RG}}} \geq 0,\ y_{it}^{\widetilde{\mathcal{RG}}} \geq 0 \tag{20b}$$

$$\Gamma_t^{\widetilde{RG}} \in [0, 1] \tag{20c}$$

Islanding event uncertainty$(\widetilde{\mathcal{I}}) - \forall t \in \Omega_T$

$$\Gamma^{\widetilde{I}} = \gamma^{\widetilde{I},Left} + \gamma^{\widetilde{I},Right} \tag{21a}$$

$$\gamma^{\widetilde{I},Left} = \sum_{t\in\Omega T} isl_t^{L}, \quad \gamma^{\widetilde{I},Right} = \sum_{t\in\Omega T} isl_t^{R} \tag{21b}$$

$$0 \leq \gamma^{\widetilde{I},Left} \leq \overline{\gamma^{\widetilde{I},Left}}, \quad 0 \leq \gamma^{\widetilde{I},Right} \leq \overline{\gamma^{\widetilde{I},Right}} \tag{21c}$$

$$0 \leq \left(I_t + isl_t^{L} + isl_t^{R}\right) \leq 1 \tag{21d}$$

$$\sum_{t\in\Omega(T)} \left(I_t + isl_t^{L} + isl_t^{R}\right) = \sum_{t\in\Omega_T} I_t + \Gamma^{\widetilde{I}} \tag{21e}$$

$$isl_t^{L} + I_t \leq isl_{t+1}^{L} + I_{t+1} \quad \forall t \leq \left(t_{start}^{isl} + \overline{\gamma^{\widetilde{I},Left}} + 1\right) \tag{21f}$$

$$isl_t^{R} + I_t \geq isl_{t+1}^{R} + I_{t+1} \quad \forall t \geq \left(t_{end}^{isl} - \overline{\gamma^{\widetilde{I},Right}} - 1\right) \tag{21g}$$

$$isl_t^{L} = 0 \quad \forall t \notin \left[t_{start}^{isl} - \overline{\gamma^{\widetilde{I},Left}} - 1,\ t_{start}^{isl} + \overline{\gamma^{\widetilde{I},Left}} + 1\right] \tag{21h}$$

$$isl_t^{R} = 0 \quad \forall t \notin \left[t_{end}^{isl} - \overline{\gamma^{\widetilde{I},Right}} - 1,\ t_{end}^{isl} + \overline{\gamma^{\widetilde{I},Right}} + 1\right] \tag{21i}$$

$$\Gamma^{\widetilde{I}} \in \left[0,\ \overline{\gamma^{\widetilde{I},Left}} + \overline{\gamma^{\widetilde{I},Right}}\right] \cap \mathbb{Z} \tag{21j}$$

$$\overline{\gamma^{\widetilde{I},Left}} = 3,\ \overline{\gamma^{\widetilde{I},Right}} = 3 \tag{21k}$$

$$\gamma^{\widetilde{I},Left},\ \gamma^{\widetilde{I},Right} \quad \text{integer} \tag{21l}$$

$$isl_t^{L},\ isl_t^{R} \quad \text{binary} \tag{21m}$$

Grid limits$-\forall t \in \Omega_T$

$$0 \leq P_t^{Grid} \leq \overline{P_t^{Grid}}\left(1 - \left(I_t + isl_t^{L} + isl_t^{R}\right)\right) \tag{22a}$$

$$0 \leq Q_t^{Grid} \leq \overline{Q_t^{Grid}}\left(1 - \left(I_t + isl_t^{L} + isl_t^{R}\right)\right). \tag{22b}$$

IV. Results and Discussion

A. Case Study and Modelling Environment

The test network used is the modified IEEE 33 bus radial distribution network following DER positioning of [5], presented in Fig. 1. Network data is extracted from [17]. DGs, ESSs, EV parking lot data are extracted from [5]. This data is given in detail in Appendix A of this article. Data granularity is 10-minute time intervals over a 24-hour scheduling horizon, i.e., $6\times24 = 144$ periods. The nominal values of the uncertain parameters are presented in Fig. 2; namely market price, renewable generation, demand, and islanding event. Total 24-hour demand is 206 MWh. Market price, renewable generation (PV), and demand uncertainty are set to $\pm10\%$ [4]. The islanding event takes place at 5pm-8pm with an hour window of uncertainty, i.e., (5pm$\pm$30 minutes)-(8pm$\pm$30 minutes). GAMS IDE environment and MOSEK solver are used for optimization problems [18]. Figures and secondary codes are produced in MATLAB R2017a and R2018a. Numerical experiments of the R-MISOCP need less than 30 seconds to run, using a desktop with an Intel Core i5-6600 CPU at 3.30 GHz and 32 GB of RAM.

In the following subsections, computational experiments are performed in order to: a) demonstrate the impacts that accuracy in power flow modelling has on scheduling decisions, and b) study the effects of adjusting the budgets of uncertainty to achieve reductions in operational cost while minimizing the probability of load shedding.

B. Power Flow Model: A Comparative Study

In this subsection, the proposed R-MISOCP model, which uses the second order cone power flow formulation of [13], is compared with an optimal MG scheduling model that uses a piecewise linear power flow formulation. The latter will be referred to as the COMP model.

As this subsection focuses on the power flow model formulation, the COMP model is compared to the R-MISOCP model results for all Γ equal to zero. The COMP model is described by the same equations as the R-MISOCP and only differs in the power flow model formulation, i.e., the COMP model does not include equations (4a)–(4h).

To preserve the comparison within day-ahead scheduling for MGs that are islanded for an extended time period, the power flow model formulation of [5] is chosen for the COMP model. The power flow model of [5] is mathematically formulated as a piecewise linear model according to [19], and the linearization follows the algorithm proposed in [20]. The power flow equations for the COMP model are formulated following these studies (i.e., [5], [19], [20]). The assumption of [5], that the voltage angles between adjacent buses $(\theta_i - \theta_j)$ range within $\pm10^{\circ}$, is preserved. The power flow formulation used for the COMP model is presented in Appendix B of this article, in equations (24a)–(24g). The remainder of this section, focuses on the impact that the power flow formulation has on the schedules and the operational costs produced by the R-MISOCP and the COMP model.

Simulation results show that the COMP model underestimates the value of network losses, compared to the R-MISOCP model. In particular, for a demand of 206 MWh, the R-MISOCP model calculates that the network losses are equal to 8.1 MWh, and the COMP model calculates that the network losses are equal to $0.0046\approx0$ MWh. Therefore, the R-MISOCP produces a generation mix that is 8.1 MWh higher than the COMP model (or 3.9% of the total demand). The different

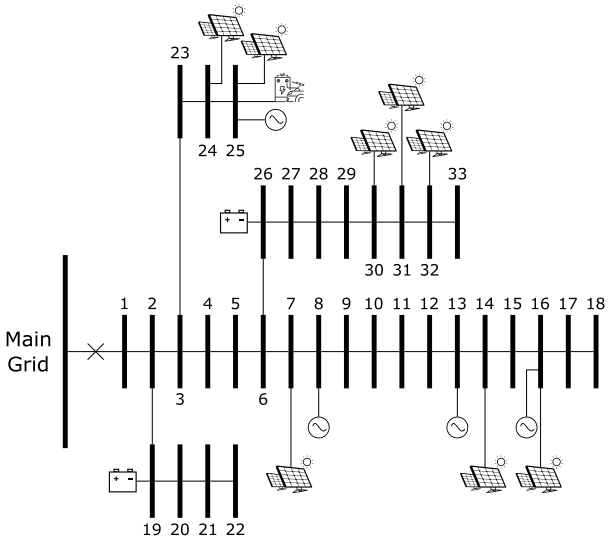

Fig. 1. Test network.

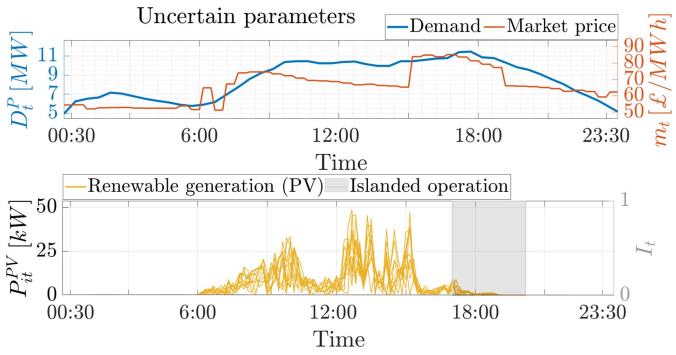

Fig. 2. Uncertain parameters. **Upper plot - Left y-axis (blue color):** Total Demand. **Upper plot - Right y-axis (red color):** Market price [21]. **Lower plot - Left y-axis (yellow color):** Renewable generation (PV). **Lower plot - Right y-axis (gray color):** Islanding duration.

calculation in network losses has also resulted in the two models calculating different schedules for the generation units and therefore different operational costs. More specifically, the R-MISOCP operational cost is £12 925, whereas the COMP operational cost is £11 443; which means, that the R-MISOCP is 11.47% more expensive than the COMP model, for the MG under study. A detailed comparison between the two models in terms of their schedules and operational costs follows below.

In Fig. 3, the main grid schedules for the R-MISOCP and COMP models are shown. During times 00:00am-06:00am, when market price is low, both models draw high levels of power from the main grid. However, a visible difference is observed between the two models (particularly during 00:00am-06:00am), as the R-MISOCP schedules a lower amount of power to be drawn from the main grid than the COMP model.

During the same period, the R-MISOCP model also prioritizes dispatching of the DGs as, although they are more expensive, they are electrically closer to the load at the given time window (Fig. 4). This is a result of the R-MISOCP model having a more accurate calculation of network losses. The demand during 00:00am-06:00am, at buses 8, 13, 16 and 25

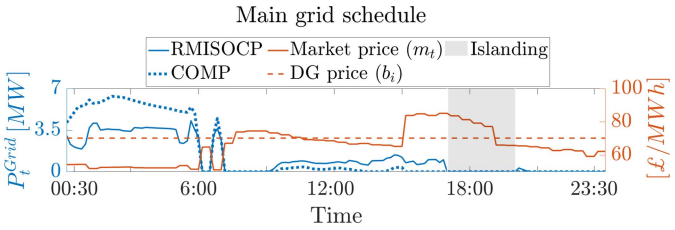

Fig. 3. **Left y-axis (blue color):** Main grid power schedule: for RMISOCP and COMP model. **Right y-axis (red color):** The market price and the cost of the dispatchable generators. The islanding event takes place between 5:00pm and 8:00pm (shown in transparent gray color).

is: 8.40 MWh, 2.52 MWh, 2.52 MWh, and 17.63 MWh respectively. Amongst all DGs, the schedule for DG at bus 8 differs significantly between the two models; this is attributed to the fact that bus 8 has a high demand, and it is located *before* the DGs at buses 13 and 16 (see Fig. 1). During the rest of the day, DG schedules remain relatively similar between the two models, as: the DG cost is lower or very close to the market price cost, DGs have reached their upper limits (Fig. 4 - Table VI), and demand is at its highest levels (Fig. 2).

Fig. 5 presents the ESS schedules for the R-MISOCP and COMP model. The ESSs are at buses 19 and 26. Bus 19 and bus 26, are both located close to the main grid bus (Fig. 1); no other generator is located between the ESSs and the main grid. ESS schedules also vary due to the calculated losses especially when discharging. In the COMP model, the dominant factor for dispatching the ESSs is market price. However, in the R-MISOCP model, the ESS schedules are affected by the occurrence of the islanding event as well (especially when discharging). This difference is noticeable between ≈3:00pm and 8:00pm (i.e., before and during the islanding event).

Fig. 6 presents the EV parking lot schedule for the R-MISOCP (continuous line) and the COMP (dotted line) model. The EV parking lot is located at bus 25, and EVs arrive at 8:30am and depart at 5:30pm (shown with two thick vertical lines at Fig. 6). Simulation results show that both models schedule the EVs according to the levels of the PV generation at bus 25 (PV generation is shown with a yellow line on the right axis of Fig. 6). More specifically, both models discharge the EVs when the PV generation is very low: which is shown after 3:00pm until 5:30pm. The R-MISOCP model mainly charges the EVs when the PV generation takes place (shown from around 12:00pm until 3:00pm with a blue line in the negative values of Fig. 6). However, the COMP model does not schedule EV charging between 8:30am and 5:30pm.

The operational cost (for both models) is the summation of: the main grid cost, the dispachable generators' cost, the load shedding cost, and the unit commitment cost. This means that the operational cost is affected, and also affects the schedules produced by the generation units. These costs are shown in Figs. 7–9 for both the R-MISOCP and the COMP model. In these figures, the left axis (blue color) presents the cumulative costs, and the right axis (red color) presents the costs per time-step.

More specifically, the fact that the COMP model schedules more power from the main grid (Fig. 3) is reflected on the cumulative main grid cost, shown in Fig. 7. Furthermore,

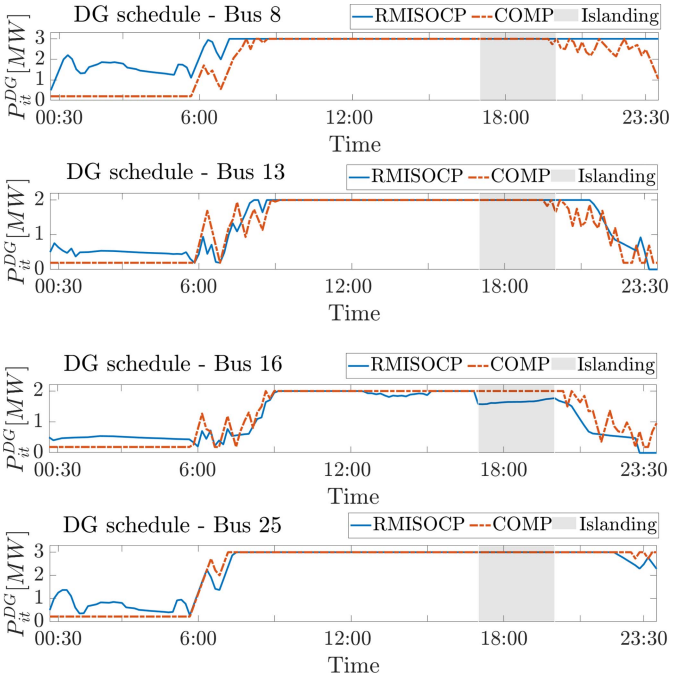

Fig. 4. Dispatchable generation schedules at buses 8, 13, 16, and 25: for RMISOCP model (blue color), and for COMP model (red color). The islanding event takes place between 5:00pm and 8:00pm (shown in transparent gray color).

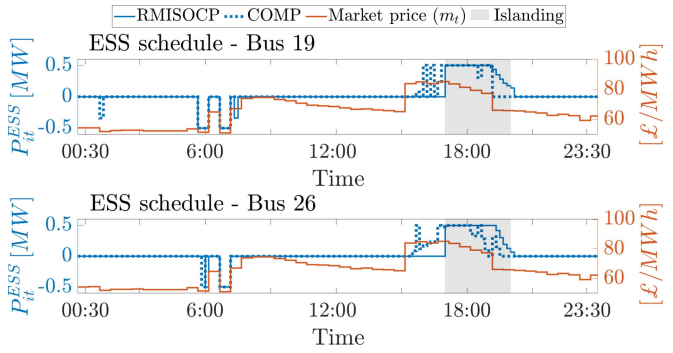

Fig. 5. ESS schedules: for bus 19 (upper plot) and for bus 26 (lower plot). **Left y-axis (blue color):** ESS schedules for the RMISOCP (continuous line) and COMP (dotted line) model. **Right y-axis (red color):** The market price. The islanding event takes place between 5:00pm and 8:00pm (shown in transparent gray color). **Positive values:** Discharge state. **Negative values:** Charge state.

the R-MISOCP model uses the dispatchable generators more than the COMP model, especially during 00:00am-06:00am (Fig. 4), which is also shown in the cumulative cost of DGs in Fig. 8.

The difference in the calculation of network losses also resulted in a lower level of load shedding by the COMP model, compared to the R-MISOCP model (Fig. 9). In particular, for a demand of 33.89 MWh during the time of the islanding (5:00pm-8:00pm), the R-MISOCP sheds 1.89 MWh and the COMP model sheds 0.2 MWh. During 5:00pm-8:00pm, the R-MISOCP calculates that network losses are equal to 1.55 MWh, whereas the COMP model calculates that losses are equal to 0.002 MWh. For a load shedding cost of $c_{i,t}^{Shed}$=£600/MWh, the cumulative cost due to load shedding,

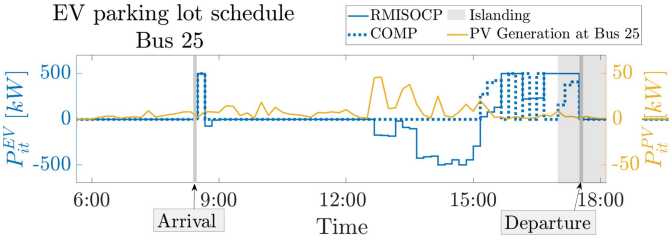

Fig. 6. EV parking lot schedule at bus 25. **Left y-axis (blue color):** RMISOCP schedule (continuous line) and COMP schedule (dotted line). **Right y-axis (yellow color):** PV generation at bus 25. The islanding event takes place between 5:00pm and 8:00pm (shown in transparent gray color). The arrival and departure of the EVs is at 8:30am and 5:30pm respectively (shown with two vertical thick gray lines). **Positive values:** Discharge state. **Negative values:** Charge state.

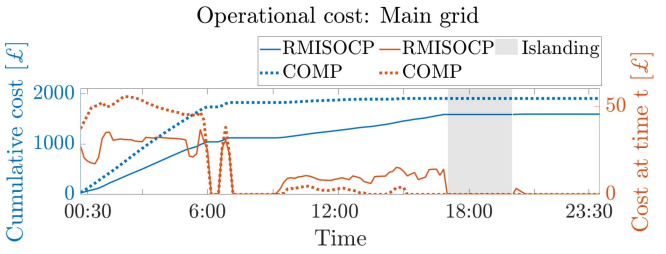

Fig. 7. **Left y-axis (blue color):** Main grid power cumulative cost for R-MISOCP and COMP models. **Right y-axis (red color):** Main grid power cost per timestep for both, R-MISOCP and COMP models. The islanding event takes place between 5:00pm and 8:00pm (shown in transparent gray color).

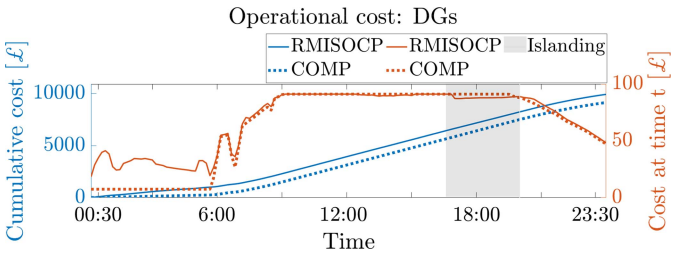

Fig. 8. **Left y-axis (blue color):** Dispatchable generation cumulative cost for R-MISOCP and COMP models. **Right y-axis (red color):** Dispatchable generation cost per timestep for both, R-MISOCP and COMP models. The islanding event takes place between 5:00pm and 8:00pm (shown in transparent gray color).

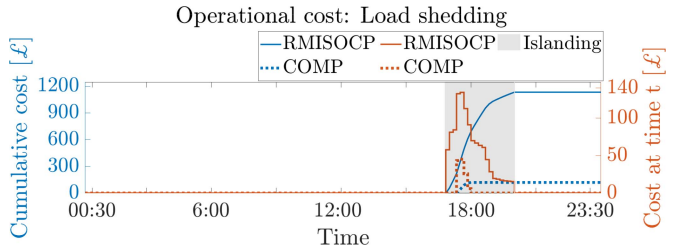

Fig. 9. **Left y-axis (blue color):** Load shedding cumulative cost for R-MISOCP and COMP models. **Right y-axis (red color):** Load shedding cost per timestep for both, R-MISOCP and COMP models. The islanding event takes place between 5:00pm and 8:00pm (shown in transparent gray color).

for both models, is shown in Fig. 9. Finally, the unit commitment cost is the same for both models, and equal to £280.1. This is expected as, for both cases, DGs start-up at 00:00am and operate continuously throughout the day (Fig. 4).

To conclude, this subsection presents a comparative study between two models that use different power flow formulations; namely, the R-MISOCP and the COMP model. Computational experiments show that the incorporation of network losses in the power flow model can impact both the operational cost and calculation of generation schedules. For the MG under study in particular, this has resulted in the following main differences between the two models. First, in terms of the operational costs, the R-MISOCP is 12% more expensive than the COMP model, since accounting for network losses in the R-MISOCP results in increased generation and increased load shedding. Second, in terms of the day-ahead schedules, the COMP model schedules, are mainly driven by the cost of generation, whereas the R-MISOCP schedule calculations, as well as the cost of generation, are also sensitive to the electrical location of the generation units.

C. Uncertainty Modelling: R-MISOCP Results

The aim of the resilience-oriented R-MISOCP model is to minimize operational costs. Operational costs include DG generation cost, unit commitment costs, main grid import costs, and the cost for load shedding. Load shedding takes place during the islanded operation if there is insufficient on-site generation to supply the demand. The four sets of uncertain data with their respective budgets of uncertainty are the following: market price with $\Gamma^{\widetilde{M}} \in [0, 144]$, demand with $\Gamma_t^{\widetilde{D}} \in [0, 1]$, renewable generation (PV) with $\Gamma_t^{\widetilde{RG}} \in [0, 1]$, and islanding duration with $\Gamma^{\widetilde{I}} \in \{0, 6\}$.

For any value of the uncertain parameters within the boundaries defined by these budgets of uncertainty, the MG operator is guaranteed that operational costs and load shedding will not exceed the values calculated by the R-MISOCP model. For example, if $\Gamma_t^{\widetilde{D}} = 0$, then no uncertainty in the values of the demand is considered, and there is no guarantee that the operational costs and load shedding will not exceed the values calculated by the R-MISOCP model. If $\Gamma_t^{\widetilde{D}} = 1$, then it is guaranteed that for any value of the demand between D_{it}^P and $D_{it}^P + 10\% D_{it}^P \ \forall i \in \Omega_B, t \in \Omega_T$, the operational costs and load shedding will not exceed the values calculated by the R-MISOCP model.

The ranges of the budgets of uncertainty for market price, demand, and renewable generation, depend on the number of uncertain parameters per constraint, as shown in [14] or Section II of this article. For example, the budget of uncertainty for market price takes values in $\Gamma_t^{\widetilde{D}} \in [0, 144]$, since there are up to 144 uncertain parameters of the market price in each constraint (16) (as this study uses 10-minute data, that result in 144 time steps). The range of the budget of uncertainty for the islanding event depends on the uncertainty in the duration of the islanding event, and represents the number of uncertain time periods. For example, if $\Gamma^{\widetilde{I}} = 6$, the islanding event duration is increased by six 10-minute time periods, i.e., the islanding event occurs between 4:30pm and 8:30pm, instead of 5:00pm-8:00pm.

However, considering the upper limits of the budgets of uncertainty can lead to conservative solutions. Therefore, the simulations below focus on how to adjust the budgets of uncertainty in order to reach a desirable trade-off between: the level of uncertainty considered, and the day-ahead operational cost and load shedding levels.

TABLE I
MODEL SENSITIVITY TO BUDGETS OF UNCERTAINTY

$\Gamma_t^{\widetilde{D}}$	$\Gamma^{\widetilde{I}}$	$\Gamma^{\widetilde{M}}$	$\Gamma_t^{\widetilde{RG}}$	Day-ahead operational cost	Load shedding [MWh]
0	0	0	0	**£12 925**	**1.89**
1	0	0	0	£15 670	4.53
0	6	0	0	£13 239	2.49
0	0	144	0	£13 024	1.89
0	0	0	1	£12 931	1.89

In this subsection, the appropriate levels of the parameters Γ are evaluated according to the probability of underestimating operational cost (PoU) and the probability of load shedding (PLS). PoU is the probability that the actual cost of operation, when considering data perturbations within the full range of uncertainty, will exceed the day-ahead operational cost calculated by the R-MISOCP model. Respectively, PLS is the probability that the actual load shedding will exceed the load shedding calculated by the R-MISOCP model, again when considering data perturbations in the full range of uncertainty. In this article, loads are shed at a cost during the islanding period. However, the MG operator can choose the budgets of uncertainty appropriately in order to ensure that this will be limited while preserving an overall low operational cost.

First, the sensitivity of the optimal day-ahead operational cost and load shedding against the four uncertain sets of data are tested. Optimal day-ahead operational cost and load shedding range from: £12 925 with 1.89 MWh, which represents <1% of total 24-hour demand, when accounting for no uncertainties (all $\Gamma = 0$); up to £16 551 with 5.89 MWh, which represents <3% of total 24-hour demand, when accounting for the full range of uncertainty (fully robust case). Therefore, the MG operator is presented with a significant range of options regarding trade-offs between the tolerance of uncertainty, and the day-ahead operational cost and load shedding levels.

According to Table I, two of the parameters that profoundly impact the day-ahead cost of operation and the load shedding are: the $\Gamma_t^{\widetilde{D}}$ for demand uncertainty, and $\Gamma^{\widetilde{I}}$ for islanding duration uncertainty. As $\Gamma^{\widetilde{M}}$ and $\Gamma_t^{\widetilde{RG}}$ do not largely affect the performance for this case, it is chosen to tolerate for these the maximum uncertainty, i.e., the maximum budgets of uncertainty are assigned for these parameters.

The levels of PoU and PLS are calculated for 21 combinations of $\Gamma_t^{\widetilde{D}} - \Gamma^{\widetilde{I}}$ (Tables II, III). The PoU and PLS are calculated by running 10 000 Monte Carlo simulations for each combination. Each iteration of the Monte Carlo simulations runs a power flow model where the inputs are: the R-MISOCP schedules (for the DGs, ESSs, and EV parking lot), and the random yields of demand spanning within its minimum and maximum limits (i.e., $D_{it}^P \pm 10\% D_{it}^P \ \forall i \in \Omega_B, t \in \Omega_T$), for $\Gamma^{\widetilde{I}} = \{0, 3 \text{ or } 6\}$. PoU is calculated as the fraction of the

TABLE II
PoU($\Gamma^{\widetilde{M}}=144$, $\Gamma_t^{\widetilde{RG}}=1$, $\Gamma^{\widetilde{D}}$, $\Gamma^{\widetilde{I}}$)

$\mathbf{\Gamma}_t^{\widetilde{D}}$	$\mathbf{\Gamma}^{\widetilde{I}}=0$	$\mathbf{\Gamma}^{\widetilde{I}}=3$	$\mathbf{\Gamma}^{\widetilde{I}}=6$ (max)
0	49.71%	49.59%	50.97%
0.001	43.46%	42.29%	42.57%
0.005	16.94%	16.51%	16.43%
0.01	3.32%	2.75%	2.62%
0.02	0.01%	0.02%	0.01%
0.03	**0%**	0%	0%
1 (max)	0%	0%	**0%**

TABLE III
PLS($\Gamma^{\widetilde{M}}=144$, $\Gamma_t^{\widetilde{RG}}=1$, $\Gamma^{\widetilde{D}}$, $\Gamma^{\widetilde{I}}$)

$\mathbf{\Gamma}_t^{\widetilde{D}}$	$\mathbf{\Gamma}^{\widetilde{I}}=0$	$\mathbf{\Gamma}^{\widetilde{I}}=3$	$\mathbf{\Gamma}^{\widetilde{I}}=6$ (max)
0	49.51%	49.71%	50.61%
0.001	45.82%	44.46%	44.30%
0.005	27.52%	25.77%	24.41%
0.01	11.55%	9.77%	8.62%
0.02	0.81%	0.49%	0.27%
0.03	**0%**	0%	0%
1 (max)	0%	0%	**0%**

TABLE IV
DAY-AHEAD COST FOR $\Gamma^{\widetilde{M}}=144$, $\Gamma_t^{\widetilde{RG}}=1$

$\mathbf{\Gamma}_t^{\widetilde{D}}$	$\mathbf{\Gamma}^{\widetilde{I}}=0$	$\mathbf{\Gamma}^{\widetilde{I}}=3$	$\mathbf{\Gamma}^{\widetilde{I}}=6$ (max)
0	£13 031	£13 169	£13 342
0.001	£13 039	£13 182	£13 351
0.005	£13 077	£13 222	£13 393
0.01	£13 123	£13 272	£13 445
0.02	£13 217	£13 371	£13 550
0.03	**£13 310**	£13 471	£13 657
1 (max)	£15 849	£16 183	**£16 551**

number of times that the actual operational cost (produced by the Monte Carlo iterations) exceeds the R-MISOCP day-ahead operational cost, over the total number of iterations. Similarly, PLS is calculated as the fraction of the number of times that the load shedding (produced by the Monte Carlo iterations) exceeds the R-MISOCP load shedding, over the total number of iterations. Power flow simulations are run using the software package of MATPOWER [22]. For the 21 combinations of $\Gamma_t^{\widetilde{D}}-\Gamma^{\widetilde{I}}$, the R-MISOCP day-ahead operational cost and load shedding values are presented in Tables IV and V respectively, and the PoU and PLS results in Tables II and III respectively.

In order to account for data perturbations in all the range of uncertainty, the MG operator would operate the MG in a fully robust case for a cost of £16 551 (Table IV), with a PoU = 0% probability of exceeding this cost during the actual operation (Table II), and a PLS = 0% probability of shedding more loads than 5.89 MWh (Tables III and V respectively). However, by selecting $\Gamma_t^{\widetilde{D}}=0.03$, $\Gamma^{\widetilde{I}}=0$, $\Gamma^{\widetilde{M}}=144$ and $\Gamma_t^{\widetilde{RG}}=1$ for the R-MISOCP model, it can be guaranteed that the load shedding will not exceed 2.13 MWh (Table V) with a probability which is also 0% (Table III), for a significantly lower operational cost of £13 310, with an also 0% probability of exceeding this cost during the actual operation (Table II).

TABLE V
LOAD SHEDDING FOR $\Gamma^{\widetilde{M}}=144$, $\Gamma_t^{\widetilde{RG}}=1$

$\mathbf{\Gamma}_t^{\widetilde{D}}$	$\mathbf{\Gamma}^{\widetilde{I}}=0$	$\mathbf{\Gamma}^{\widetilde{I}}=3$	$\mathbf{\Gamma}^{\widetilde{I}}=6$ (max)
0	1.88 MWh	2.15 MWh	2.49 MWh
0.001	1.89 MWh	2.17 MWh	2.50 MWh
0.005	1.93 MWh	2.20 MWh	2.54 MWh
0.01	1.97 MWh	2.25 MWh	2.59 MWh
0.02	2.05 MWh	2.34 MWh	2.69 MWh
0.03	**2.13 MWh**	2.44 MWh	2.80 MWh
1 (max)	4.52 MWh	5.17 MWh	**5.89 MWh**

V. CONCLUSION

This article presents a Robust Mixed-Integer Second Order Cone Programming model for the day-ahead scheduling of MicroGrids that are islanded for an extended and uncertain period of time due to a power interruption from the main grid. The R-MISOCP model holds the benefits of both convexity and robustness.

In terms of the power flow formulation used in this work, it is shown that incorporation of a non-accurate AC power flow model (that does not account for network losses), can result in a sizable underestimation of the day-ahead operational cost; as accounting for network losses in the power flow model, results in higher generation and increased load shedding. For the MG under study, comparing the proposed model with a model that uses a piecewise linear power flow formulation, this underestimation is found to be 11.47%. Furthermore, it is shown that when network losses are not taken into account, the scheduling decisions are mainly driven by the cost of generation units; whereas, when accounting for network losses, the scheduling decisions are sensitive to both the cost of generation units and their electrical location within the network. In terms of the uncertainty modelling, it is shown with the R-MISOCP model that the MG operator can achieve a significant trade-off between tolerance of data perturbations of the uncertain data, and performance. In particular, computational experiments show that by adjusting the budgets of uncertainty, the MG operator can achieve a 19.58% reduction in the day-ahead operational cost, compared to a fully robust schedule. Moreover, the R-MISOCP model can guarantee 54.33% lower load shedding compared to a fully robust schedule, while preserving a 0% probability of additional load shedding during the actual operation.

TABLE VI
DG TECHNICAL CONSTRAINTS [5]

Bus	$\underline{P_{it}^{DG}}$ [MW]	$\overline{P_{it}^{DG}}$ [MW]	$\underline{Q_{it}^{DG}}$ [MVar]	$\overline{Q_{it}^{DG}}$ [MVar]	b_i [£/MWh]	a_i [£]
8	0.21	3	-2.1	2.1	70.20	0
13	0.19	2	-1.9	1.9	70.20	0
16	0.19	2	-1.9	1.9	70.20	0
25	0.22	3	-2.2	2.2	70.20	0

TABLE VII
ESS TECHNICAL CONSTRAINTS [5]

Bus	C_i^{max} [MWh]	$SOC_{i(t=1)}$, $SOC_{i(t=T_{max})}$ [%]	$\overline{P_{it}^{ESS,Ch}}$ [MW]	$\overline{P_{it}^{ESS,Disch}}$ [MW]
19	1.5	66.6	0.5	0.5
26	1.5	80	0.5	0.5

TABLE VIII
EV PARKING LOT TECHNICAL CONSTRAINTS [5]

Bus	$\overline{E_{EV}}$ [MW]	$\overline{P_{it}^{EV}}$ [MWh]	soc_i^{arr} [%]	soc_i^{dep} [%]	SOC_{it}^{Sat} [%]	$T_{arr} - T_{dep}$ [period]
25	2	0.5	10	50	85	51 - 105 (8:30am - 5:30pm)

Two general points to discuss are in order. Firstly, the proposed approach is designed for MGs. However, it can also be used for radial distribution networks with distributed energy resources and Active Distribution Networks. Furthermore, the proposed method is applicable to business-as-usual case studies, with no islanding event, by setting $I_t = 0 \, \forall \, t$. Secondly, the proposed R-MISOCP model can be reformulated to a mixed-integer linear programming problem using the ϵ-polyhedral approximation of [23] with a very high accuracy. This ability can be found very useful, particularly for studies where, mathematically, a linear model formulation is preferable.

APPENDIX A
DATA

This Appendix presents the data introduced in Section IV-A. The DG, ESS and EV parking lot technical constraints are shown in Tables VI, VII, VIII respectively. Branch data are shown in Table IX.

APPENDIX B
PIECEWISE LINEAR POWER FLOW MODEL (PWL-PF)

This section presents the PWL-PF model formulation of the COMP model, used in Section IV-B. For completeness, the non-convex formulation of the piecewise linear power flow model is first presented, and subsequently the piecewise linear formulation (PWL-PF).

The non-convex formulation of the power flow model formulation used in [5] is shown in equations (23a)–(23b) below.

TABLE IX
NETWORK DATA [17]

Branch	r_{ij} [Ω]	x_{ij} [Ω]	Branch	r_{ij} [Ω]	x_{ij} [Ω]
1 - 2	0.0922	0.0470	17 - 18	0.7320	0.5740
2 - 3	0.4930	0.2511	2 - 19	0.1640	0.1565
3 - 4	0.3660	0.1864	19 - 20	1.5042	1.3554
4 - 5	0.3811	0.1941	20 - 21	0.4095	0.4784
5 - 6	0.8190	0.7070	21 - 22	0.7089	0.9373
6 - 7	0.1872	0.6188	3 - 23	0.4512	0.3083
7 - 8	0.7114	0.2351	23 - 24	0.8980	0.7091
8 - 9	1.0300	0.7400	24 - 25	0.8960	0.7011
9 - 10	1.0440	0.7400	6 - 26	0.2030	0.1034
10 - 11	0.1966	0.0650	26 - 27	0.2842	0.1447
11 - 12	0.3744	0.1238	27 - 28	1.0590	0.9337
12 - 13	1.4680	1.1550	28 - 29	0.8042	0.7006
13 - 14	0.5416	0.7129	29 - 30	0.5075	0.2585
14 - 15	0.5910	0.5260	30 - 31	0.9744	0.9630
15 - 16	0.7463	0.5450	31 - 32	0.3105	0.3619
16 - 17	1.2890	1.7210	32 - 33	0.3410	0.5302

$$PF_{ij,t}^{P} = g_{ij}\left(V_{it}^2 - V_{it}\,V_{jt}\,\cos\left(\theta_{it} - \theta_{jt}\right)\right) - b_{ij}\left(V_{it}\,V_{jt}\,\sin\left(\theta_{it} - \theta_{jt}\right)\right) \quad \forall (i,j) \in E \quad \forall t \in \Omega_T \tag{23a}$$

$$PF_{ij,t}^{Q} = -b_{ij}\left(V_{it}^2 - V_{it}\,V_{jt}\,\cos\left(\theta_{it} - \theta_{jt}\right)\right) - g_{ij}\left(V_{it}\,V_{jt}\,\sin\left(\theta_{it} - \theta_{jt}\right)\right) \quad \forall (i,j) \in E \quad \forall t \in \Omega_T \tag{23b}$$

According to [5], [19], [20], equation (23a) is linearized to (24a), and equation (23b) is linearized to (24b), as shown below.

$$PF_{ij,t}^{P} = g_{ij}\left(V_{it} - V_{jt} - \omega_{ij,t}^{PWL} + 1\right) - b_{ij}\left(\theta_{it} - \theta_{jt}\right) \quad \forall (i,j) \in E \quad \forall t \in \Omega_T \tag{24a}$$

$$PF_{ij,t}^{Q} = -b_{ij}\left(V_{it} - V_{jt} - \omega_{ij,t}^{PWL} + 1\right) - g_{ij}\left(\theta_{it} - \theta_{jt}\right) \quad \forall (i,j) \in E \quad \forall t \in \Omega_T \tag{24b}$$

The term $\cos\left(\theta_{it} - \theta_{jt}\right)$ of equations (23a)-(23b) is approximated by the linear segments shown in (24c), using the algorithm proposed in [20] for the calculation of the terms h_n and d_n.

$$\omega_{ij,t}^{PWL} \leq h_n\left(\theta_{it} - \theta_{jt}\right) + d_n \quad \forall (i,j) \in E \quad \forall t \in \Omega_T \quad \forall n \tag{24c}$$

where n is the number of linear inequalities used to approximate the $\cos\left(\theta_{it} - \theta_{jt}\right)$. The piecewise linearization of $\cos\left(\theta_{it} - \theta_{jt}\right)$ for $|\theta_{it} - \theta_{jt}| \leq 10°$ (following the study in [5]), is shown in Fig. 10 for seven linear segments.

Along with equations (24a)–(24c), the COMP model power flow formulation is also comprised of the following equations:

$$\sum_{j:(i,j)\in E} PF_{ij,t}^{P} = G_{it}^{P} - D_{it}^{P} \tag{24d}$$

$$\sum_{j:(i,j)\in E} PF_{ij,t}^{Q} = G_{it}^{Q} - D_{it}^{Q} \tag{24e}$$

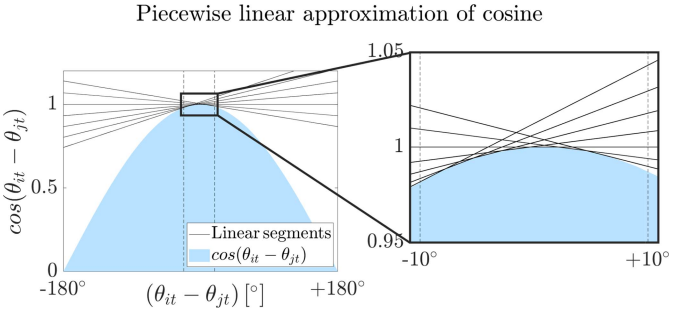

Fig. 10. Piecewise linearization of $\cos(\theta_{it}-\theta_{jt})$ for $|\theta_{it}-\theta_{jt}| \leq 10°$ using seven linear segments.

$$PF^{P}_{ij,t} + PF^{P}_{ji,t} \leq PF^{loss}_{ij} \tag{24f}$$

$$PF^{loss}_{ij} = \frac{g_{ij}}{g^2_{ij}+b^2_{ij}}\overline{I_{ij}} \tag{24g}$$

where, (24d) and (24e) are the real and reactive power flow balance respectively, and (24f)–(24g) represent the feeder loss, which is comprised of the summation of the active power injections [5].

ACKNOWLEDGMENT

Data supporting this publication are available at https://doi.org/10.25405/data.ncl.13235516.

REFERENCES

[1] J. A. P. Lopes, C. L. Moreira, and A. G. Madureira, "Defining control strategies for microgrids islanded operation," *IEEE Trans. Power Syst.*, vol. 21, no. 2, pp. 916–924, May 2006.
[2] F. Katiraei and M. R. Iravani, "Power management strategies for a microgrid with multiple distributed generation units," *IEEE Trans. Power Syst.*, vol. 21, no. 4, pp. 1821–1831, Nov. 2006.
[3] N. Hatziargyriou, *The Microgrids Concept*. Hoboken, NJ, USA: Wiley, 2014.
[4] A. Khodaei, "Resiliency-oriented microgrid optimal scheduling," *IEEE Trans. Smart Grid*, vol. 5, no. 4, pp. 1584–1591, Jul. 2014.
[5] A. Gholami, T. Shekari, F. Aminifar, and M. Shahidehpour, "Microgrid scheduling with uncertainty: The quest for resilience," *IEEE Trans. Smart Grid*, vol. 7, no. 6, pp. 2849–2858, Nov. 2016.
[6] A. Gholami, T. Shekari, and S. Grijalva, "Proactive management of microgrids for resiliency enhancement: An adaptive robust approach," *IEEE Trans. Sustain. Energy*, vol. 10, no. 1, pp. 470–480, Jan. 2019.
[7] Z. Li, M. Shahidehpour, F. Aminifar, A. Alabdulwahab, and Y. Al-Turki, "Networked microgrids for enhancing the power system resilience," *Proc. IEEE*, vol. 105, no. 7, pp. 1289–1310, Jul. 2017.
[8] X. Liu, M. Shahidehpour, Z. Li, X. Liu, Y. Cao, and Z. Bie, "Microgrids for enhancing the power grid resilience in extreme conditions," *IEEE Trans. Smart Grid*, vol. 8, no. 2, pp. 589–597, Mar. 2017.
[9] Y. Wang, C. Chen, J. Wang, and R. Baldick, "Research on resilience of power systems under natural disasters—A review," *IEEE Trans. Power Syst.*, vol. 31, no. 2, pp. 1604–1613, Mar. 2016.
[10] A. Hussain, V.-H. Bui, and H.-M. Kim, "A proactive and survivability-constrained operation strategy for enhancing resilience of microgrids using energy storage system," *IEEE Access*, vol. 6, pp. 75495–75507, 2018.
[11] Y. Guo and C. Zhao, "Islanding-aware robust energy management for microgrids," *IEEE Trans. Smart Grid*, vol. 9, no. 2, pp. 1301–1309, Mar. 2018.
[12] K. Balasubramaniam, P. Saraf, R. Hadidi, and E. B. Makram, "Energy management system for enhanced resiliency of microgrids during islanded operation," *Electric Power Syst. Res.*, vol. 137, pp. 133–141, Aug. 2016.
[13] M. Farivar and S. H. Low, "Branch flow model: Relaxations and convexification—Part I," *IEEE Trans. Power Syst.*, vol. 28, no. 3, pp. 2554–2564, Aug. 2013.
[14] D. Bertsimas and M. Sim, "The price of robustness," *Oper. Res.*, vol. 52, no. 1, pp. 35–53, 2004.
[15] D. Bertsimas, D. B. Brown, and C. Caramanis, "Theory and applications of robust optimization," *SIAM Rev.*, vol. 53, pp. 464–501, Aug. 2011.
[16] S. I. Vagropoulos and A. G. Bakirtzis, "Optimal bidding strategy for electric vehicle aggregators in electricity markets," *IEEE Trans. Power Syst.*, vol. 28, no. 4, pp. 4031–4041, Nov. 2013.
[17] M. Baran and F. F. Wu, "Optimal sizing of capacitors placed on a radial distribution system," *IEEE Trans. Power Del.*, vol. 4, no. 1, pp. 735–743, Jan. 1989.
[18] *Mosek Modeling Cookbook*, MOSEK ApS, Copenhagen, Denmark, 2019.
[19] P. A. Trodden, W. A. Bukhsh, A. Grothey, and K. I. M. McKinnon, "Optimization-based islanding of power networks using piecewise linear AC power flow," *IEEE Trans. Power Syst.*, vol. 29, no. 3, pp. 1212–1220, May 2014.
[20] C. Coffrin and P. Van Hentenryck, "A linear-programming approximation of AC power flows," *INFORMS J. Comput.*, vol. 26, pp. 645–914, Jun. 2012.
[21] *System Sell and System Buy Prices*, ELEXON, London, U.K., 2019.
[22] R. D. Zimmerman, C. E. Murillo-Sanchez, and R. J. Thomas, "MATPOWER: Steady-state operations, planning, and analysis tools for power systems research and education," *IEEE Trans. Power Syst.*, vol. 26, no. 1, pp. 12–19, Feb. 2011.
[23] A. Ben-Tal and A. Nemirovski, "On polyhedral approximations of the second-order cone," *Math. Oper. Res.*, vol. 26, pp. 193–205, May 2001.

Natalia-Maria Zografou-Barredo received the Diploma degree from the Department of Electrical and Computer Engineering, School of Engineering, University of Patras, Greece, in 2016. She is currently pursuing the Ph.D. degree in electrical and electronic engineering with the School of Engineering, Newcastle University, U.K.

Her current research interests include distribution network operation, active network management, microgrid operation, and mathematical optimization.

She is the recipient of the 2016 IEEE Greece Power and Energy Society POWERED Award (16th Workshop on Power Engineering Dissertations).

Charalampos Patsios (Member, IEEE) is a Senior Lecturer with Power Systems with a significant experience in the design, modeling, and control of power systems including renewables. He is the Co-Director and the WP Leader for the Supergen Energy Storage Network+, and the Work Package Leader for the £5m EPSRC's National Center for Energy Systems Integration. His research focuses on the development of integrated models and control techniques for flexibility resources such as energy storage in modern networks, working closely with U.K. industry and academia on a number of research projects and initiatives.

Ilias Sarantakos received the Dipl.Ing. degree from the School of Electrical and Computer Engineering, National Technical University of Athens, Greece, in 2013, and the Ph.D. degree from the School of Engineering, Newcastle University, U.K., in 2019.

Since 2018, he has been a Postdoctoral Researcher with the Electrical Power Research Group, Newcastle University. His research interests include distribution network operation and planning, optimization, reliability, and security of supply.

Peter Davison received the B.Eng. and M.Sc. degrees from Durham University, U.K., in 2010 and 2011, respectively, and the Ph.D. degree from Newcastle University, U.K., in 2017. His research interests include smart grids, dynamic line ratings, and novel demand side response techniques.

Sara Louise Walker received the B.Sc. degree (Hons.) in physics from Leicester University in 1991, the Post Graduate Certificate in education from Leicester University in 1992, the M.Sc. degree in environmental science from Nottingham University in 1994, and the Ph.D. degree in energy from De Montfort University in 2003. Her employment experience includes a period of Teaching in secondary education, research, and Teaching with De Montfort University, five years in industry with IT Power Ltd and Econnect Ltd, and two further academic roles with Northumbria University as Principal Lecturer and now with Newcastle University as Reader in energy. She is the Director of the EPSRC National Center for Energy Systems Integration, and as a Senior Fellow of the U.K. Higher Education Academy.

Philip C. Taylor (Senior Member, IEEE) was appointed as the Pro Vice-Chancellor for Research and Enterprise with the University of Bristol in summer 2020. He is an internationally leading Researcher and an Industrial expert in energy systems, who has worked in industry and academia for over 25 years. He joined Newcastle University in 2013, as a Dean and the Director of the Multidisciplinary Institute for Sustainability, and later, became the Head of the School of Engineering. He is currently the Co-Director of the £20m EPSRC National Center for Energy Systems Integration and also the Director of the £10m EPSRC Supergen Energy Networks Hub, which brings together industrial and academic partners (including five U.K. universities) with other energy network stakeholders. His work in industry includes time with GEC Alstom, EPS, U.K., Teradyne, and Senergy Econnect. He is a Member of the Board of Trustees for National Energy Action, a fuel poverty charity. In addition to being a Visiting Professor with Nanyang Technological University, Singapore, he is also a Non-Executive Director of Northern Powergrid, an electrical distribution company, which provides power to eight million customers in the North East and Yorkshire.